NASA CONTRACTOR REPORT

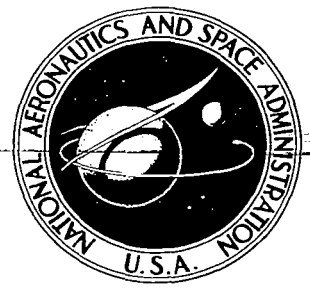

NASA CR-3

NASA CR-358

BEHAVIOR OF THE SONIC BOOM SHOCK WAVE NEAR THE SONIC CUTOFF ALTITUDE

by Manfred P. Friedman and David C. Chou

Prepared under Contract No. NAS 1-2511 *by*
MASSACHUSETTS INSTITUTE OF TECHNOLOGY
Cambridge, Mass.
for Langley Research Center

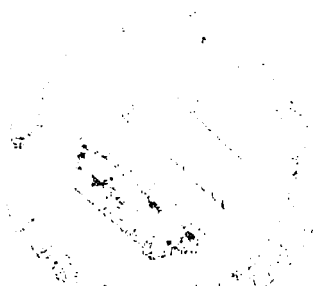

NATIONAL AERONAUTICS AND SPACE ADMINISTRATION • WASHINGTON, D. C. • DECEMBER 1965

NASA CR-358

BEHAVIOR OF THE SONIC BOOM SHOCK WAVE NEAR THE SONIC CUTOFF ALTITUDE

By Manfred P. Friedman and David C. Chou

Prepared under Contract No. NAS 1-2511 by
MASSACHUSETTS INSTITUTE OF TECHNOLOGY
Cambridge, Mass.

for Langley Research Center

NATIONAL AERONAUTICS AND SPACE ADMINISTRATION

For sale by the Clearinghouse for Federal Scientific and Technical Information
Springfield, Virginia 22151 – Price $3.00

FOREWORD

The work done on this project was supported by NASA, Contract NAS 1-2511. All of the computer work was done at the Computation Center at MIT, Cambridge, Massachusetts.

ABSTRACT

A detailed description is presented of the behavior of a sonic boom shock wave near the sonic cutoff altitude, at this altitude the local sound speed is equal to the aircraft speed. The analysis being based on a model atmosphere in which sound decreases linearly with altitude. It is shown that existing theories using geometrical acoustic ray tube concepts do not correctly describe the situation near cutoff. As the shock first propagates away from the aircraft its strength decreases. However, as it approaches a region where the flow behind the shock is transonic the pressure jump across the shock increases, despite the fact that the Mach number is decreasing. The pressure jump increase is caused by accumulated disturbances behind the shock which are unable to propagate away in this transonic flow region. When the flow behind the shock is fully subsonic the pressure jump again decrease, the shock finally ending, at zero strength, embedded in a compression wave. A very interesting result is that in the vicinity of the altitude at which the shock disappears, compression signals from the aircraft arrive ahead of the bow wave.

TABLE OF CONTENTS

LIST OF ILLUSTRATIONS

LIST OF SYMBOLS

a	sound speed at aircraft altitude
a'	$a - k(z - h)$ = atmospheric sound speed
a^*	perturbed sound speed, see Section IV.1
A	adjusted sound speed, see Section IV.2
h	aircraft altitude
k	sound speed gradient
M	Mach number
n_i	$(i = 1, 2, 3)$; x, y, z components of normal to characteristic surface
ΔN	distance between characteristic surfaces at times t and $t + \Delta t$
p	pressure
s	distance along ray
t	time
T	time measured after τ
U	aircraft velocity
u_i	$(i = 1, 2, 3)$; x, y, z components of velocity
u	horizontal velocity, in x direction
w	vertical velocity, in z direction
x_i	$(i = 1, 2, 3)$; x, y, z
x	horizontal coordinate in flight path direction
y	horizontal lateral coordinate
z	vertical coordinate
α	parameter in adjusted sound speed, Eqs. (IV.12), (IV.14)
β	parameter in adjusted sound speed, Eqs. (IV.12), (IV.15)

LIST OF SYMBOLS (Continued)

γ	ratio of specific heats
ϵ	initial ray inclination from horizontal
λ	$T - \tau$, time measured after τ
ω	angle between a vertical plane and the x, z plane
ρ	density
θ	shock inclination from horizontal
θ_h	shock inclination at aircraft altitude
ψ	wave front perturbation
ϕ	characteristic surface
Φ	perturbed wave front surface
τ	time of disturbance initiation
η	sound speed perturbation
ξ_k	(k = 0, 1, 2, 3) direction cosine, Eq. (A-2)

CHAPTER I

INTRODUCTION

The purpose of this study is to determine the behavior of the sonic boom shock wave when it arrives in the neighborhood of the sonic cutoff altitude. At this altitude the local sound speed is equal to the aircraft speed. This occurs below the aircraft for low supersonic Mach number ($1 < M < 1.2$) flights; and is due to the fact that sound speed decreases by about 20 percent with increasing altitude over a range of 0 to 50,000 ft.

The approach used here depends strongly on acoustical concepts for the following reasons:

(1) The nonlinear theory developed by Whitham (Refs. 1, 2) is, for the most part, inapplicable for describing details of the present problem (this will be discussed in the body of the report).

(2) Many of the mathematical equations describing the location and properties of the disturbance wave fronts can be given explicitly for the case in which sound speed varies linearly with altitude (Refs. 3, 5). Furthermore, this model of the atmosphere gives an accurate description of a standard atmosphere and it also permits an adequate description of all relevant physical phenomena.

(3) The boom is quite weak in the regions considered, having a pressure ratio, $\Delta p/p$, of order .001. Therefore it is slightly more than a sound wave.

(4) It is quite important to give the shape of the shock wave and its location relative to the ambient atmosphere. Satisfactory results have been obtained for shock location techniques (Refs. 3, 4, 5) which are based either on acoustical ray or wave front tracing.

We shall assume in the remainder of this report that the boom was caused by an aircraft in straight horizontal flight, and that the sound speed decreases linearly with increasing altitude between the ground and 35,000 ft. In addition, the effects of winds are neglected.

As a shock wave propagates through a "standard" atmosphere it goes through various phases depending on its inclination and the incoming flow Mach number. If we locate a reference coordinate system on the shock we notice that the incoming flow has a constant velocity, equal to the aircraft velocity, but a Mach number which decreases with decreasing altitude. As we move down the shock, toward the ground, it becomes vertical near the sonic altitude. We define the initial phase, Region 1 of Fig. 1, to be where the flows both ahead of and behind the shock are supersonic. Here, except very near the bottom end of Region 1, the theories developed by Whitham, Refs. 1, 2, and extended in Ref. 4 are applicable. In Region 2 (Fig. 1) there is supersonic flow upstream of the shock and subsonic flow downstream. Here again, except in the vicinity of the boundary between Regions 1 and 2, the theory of Ref. 4 is applicable. Therefore the theory of Ref. 4 gives an adequate description of the shock strength except for those situations when the flow behind the shock is near sonic. In Region 3 (Fig. 1) there is no shock. It will be shown that here there is only a series of compression waves similar to those occurring below a subsonic aircraft.

Of interest in these considerations is the pressure ratio, $\Delta p/p$, across the shock. As we move down through Region 1 the pressure ratio decreases as predicted in Refs. 1, 2, 4. However, very near the end of Region 1 the pressure ratio starts to increase, despite the fact that the incoming flow Mach number is decreasing. This behavior is not predicted in Refs. 1, 2, 4; it is, however, indicated in an analysis by Moeckel in Ref. 6. A technique similar to, but simpler than, Moeckel's is developed later in this report. Lighthill, Ref. 7 page 317, also mentions (without proof) that the pressure ratio increases as the shock approaches the transonic (behind the shock) region. This pressure increase is caused by two complimentary phenomena. First there is a focusing of the wave energy emitted by the aircraft; one can see in Fig. 2 that many pressure wave fronts simultaneously arrive in this region. Second, in the transonic region behind the shock both the characteristics and the shock itself are nearly vertical. Therefore pressure disturbances created by the shock propagate upward and downward, all remaining in the immediate vicinity of the

shock. These tend to accumulate and give rise to higher than expected overpressures.

In Region 2, where the flow behind the shock is subsonic, the complete flow field ahead of and behind the shock is quite complicated. The major cause for this complication is the fact that in the lower part of this region disturbances, caused by the aircraft, arrive before the bow wave; i.e., there is a compression field in front of the bow shock. However, since the shock is formed (or ends, depending upon how you consider the situation) in this compression field its strength here is quite small, tending to zero. The overall pressure increase here is due to the combination shock plus pressure field.

Below Region 2, in Region 3, the flow is everywhere subsonic. Here there is no abrupt pressure increase and hence no boom, the pressure is spread out into a continuous rise. What is experienced in this region is a loud rumble such as would be caused by a subsonic aircraft.

In Chapter II relevant acoustical equations and a description of the flow field, based on these equations, is presented. It is shown how the subsonic flow of Region 3 (Fig. 1) is connected with the supersonic flow at higher altitudes. In Chapter III a theory paralleling that of Moeckel (Ref. 6) is presented. We show here that the pressure jump across the shock can increase while the shock Mach number decreases. In Chapter IV some extensions to the acoustical theory are given. Finally, in Chapter V the results are reviewed, and the lateral propagation problem is discussed.

CHAPTER II

CHARACTERISTICS, WAVE FRONTS AND RAYS

II.1 ACOUSTIC WAVE FRONTS AND RAYS

It is shown in Appendix A, Eq. (A8), that characteristic surfaces for unsteady Eulerian flow equations satisfy the partial differential equation

$$\phi_t + u_i \phi_{x_i} \pm a \sqrt{\phi_{x_i} \phi_{x_i}} = 0 \qquad \text{(II.1)}$$

We will now show that this is also the equation for the acoustic wave fronts, and therefore that the acoustic wave fronts are characteristic surfaces. We will also show that for steady supersonic flows Eq. (II.1) can be reduced to the equation for the Mach lines. This relation between the acoustic wave fronts, which exist independent of the flow speed, and the supersonic Mach lines will be used in Section II.3 to connect the flow in Regions 2 and 3 of Fig. 1.

At any time, t, $\phi(t, x_i) = 0$ gives the location of the characteristic surface in cartesian $x_i = x, y, z$ space. At time $t + \Delta t$ the surface will be at $\phi(t + \Delta t, x_i + n_i \Delta N) = 0$, where $n_i(x, y, z)$ is the direction cosine of the surface normal and $\Delta N(x, y, z)$ is the perpendicular distance between $\phi(t, x_i) = 0$ and $\phi(t + \Delta t, x_i + n_i \Delta N) = 0$. Expanding the latter equation about (t, x_i) leads to

$$\Delta N n_i \phi_{x_i} + \Delta t \phi_t = 0$$

or

$$\frac{dN}{dt} = - \frac{\phi_t}{n_i \phi_{x_i}} = - \frac{\phi_t}{\sqrt{\phi_{x_i} \phi_{x_i}}} \qquad \text{(II.2)}$$

where we have used the definition of n_i

$$n_i = \phi_{x_i} / \sqrt{\phi_{x_i} \phi_{x_i}} \qquad \text{(II.3)}$$

Substituting Eqs. (II.2) and (II.3) into (II.1)

$$\frac{dN}{dt} - u_i n_i = \pm a \tag{II.4}$$

Equation (II.4) shows that the characteristic surface moves at sound speed relative to the local flow, in a direction normal to itself. This, however, is exactly the definition of the acoustic wave fronts, therefore the characteristic surfaces given by Eq. (II.1) are also acoustic wave fronts. Since we are considering disturbances which propagate outward from some initial point Eqs. (II.1) and (II.4) will be taken with the + sign in the remainder of this report.

The equations for acoustical rays, along which the wave fronts propagate, have been derived in Refs. 3 and 4 and will not be rederived here. For the special case of linear sound speed variation the ray and the wave front equations can be solved exactly; see, e.g. Refs. 3 and 5. Solutions will be given here in terms x, z (horizontal, vertical) coordinates since we will be considering flow behavior in the vertical plane containing the aircraft. (A discussion of lateral propagation effects will be presented later in the report.)

Ray Equation

$$x = -U(T-\tau) + \frac{a}{k}\left\{\tan\epsilon \pm \sqrt{\sec^2\epsilon - \left(\frac{a'}{a}\right)^2}\right\} \tag{II.5}$$

Wave Front Equation

$$x = -U(T-\tau) + \frac{a}{k}\sqrt{\frac{2a'}{a}\cosh k(T-\tau) - \left(\frac{a'}{a}\right)^2 - 1} \tag{II.6}$$

where $a' = a - k(z-h)$ (II.7)

The last equation gives the linear variation of sound speed a' versus altitude z, in several of the equations involving rays or wave fronts we will use a' instead of z, they are simply related through Eq. (II.7); a is sound speed at aircraft altitude h; k (.004 sec^{-1} for a standard atmosphere) the sound speed gradient. τ is the time when the disturbance was created, T is time measured after τ, ϵ is the initial ray angle measured

positive downward from the horizontal axis.

These equations have been written in a coordinate system fixed with respect to the aircraft, which is located at x = 0, z = h and is headed along the positive x direction. In this coordinate system the wave front differential Eq. (II.1) becomes

$$\phi_T - U\phi_x + a'\sqrt{\phi_x^2 + \phi_z^2} = 0 \qquad \text{(II.8)}$$

The above Eqs. (II.5)-(II.8) are linearized in the sense that small velocity and sound speed perturbations, caused by the aircraft, are neglected. However, the variation of sound speed with altitude is retained. In Whitham's original paper, Ref. 1, the perturbations are included but sound speed variation in neglected. Since we are mainly interested in the acoustic cutoff problem we must retain the sound speed variation with altitude.

II.2 FLOW FIELD DESCRIPTION BASED ON ACOUSTIC WAVE FRONTS

In Figs. 2a and 2b we have drawn several wave fronts as given by Eq. (II.6). The first thing to be noted is that these wave fronts form an envelope above and below the aircraft. In addition the envelope below the aircraft has a cusp at the sonic altitude and is reflected upward Because of the density of wave front lines the bow wave construction is given in Fig. 2a, and the reflected wave after the cusp in Fig. 2b. The equation for the wave front envelope can be found by differentiating Eq. (II.6) with respect to τ, and setting $dx/d\tau = 0$. It is most clearly presented by letting $T - \tau$ be parametrically dependent on z or vice versa:

$$\cosh k\lambda = \frac{U^2}{a\,a'} \pm \sqrt{\left(\left(\frac{U}{a}\right)^2 - 1\right)\left(\left(\frac{U}{a'}\right)^2 - 1\right)} \qquad \text{(II.9)}$$

or

$$\frac{a'}{a} = \left\{\cosh k\lambda - \sqrt{1 - \left(\frac{a}{U}\right)^2}\,\sinh k\lambda\right\}^{-1} \qquad \text{(II.10)}$$

where

$$\lambda = T - \tau,\quad a' = a - k\,(z - h)$$

We will only consider wave fronts below the aircraft, therefore initially the minus sign is taken in Eq. (II.9). As we move downward both λ and a' increase, as indicated in Eq. (II.10). At the altitude corresponding to $a' = U$ the square root in (II.9) vanishes and from then on the plus sign is taken. As λ continues to increase a' starts decreasing, we are now on the reflected shock front, Fig. 2b. For every value of z and λ the x coordinate of the shock front is found from Eq. (II.6).

For the purpose of some later discussions we take a brief digression here. The basic, steady flight, problem which we are considering is time invariant. Therefore the time parameter $\lambda = T - \tau$ is actually only a characteristic parameter which is used only to identify different characteristic surfaces. Equations (II.9) and (II.10) identify z and λ along the shock front. These equations consider the flow at time T; for each altitude z on the shock front there corresponds a wave front which originated at the flight path at time τ. Therefore Eqs. (II.9) and (II.10) along the shock front relate z and τ if we hold T fixed. If, however, we hold τ fixed and assume T varies ($T > \tau$) these equations give the altitude of the ray which left the flight path at time τ and at angle $\epsilon = 90° - \mu$, where $\mu = \sin^{-1}(1/M)$ is the Mach angle. Therefore Eqs. (II.9) and (II.10) can be used along the ray $\epsilon = 90° - \mu$. In general, for any ray leaving at angle ϵ the altitude z given as a function of time T after departure is

$$\frac{a'}{a} = \left\{\cosh k\lambda - \sin\epsilon \sinh k\lambda\right\}^{-1} \qquad \text{(II.11)}$$

Although Eqs. (II.5) to (II.10) are based on linearized theory a considerable amount of information can be obtained from them. In fact they contain the essence of the problem. First the bow wave, represented by the envelope of the wave fronts, has associated with it a reflected shock wave and therefore in a small region near the cutoff altitude there are two shocks very near to each other. These shocks being caused by similar signals are approximately the same strength. (It is doubtful that the reflected shock actually exists since the flow behind the bow shock is subsonic near the sonic altitude. The pressure disturbances overtake and merge with the bow shock resulting in a reinforced bow wave). Therefore measured overpressures here would be about twice the value predicted across the single shock bow wave.

Next, a close examination of the acoustic wave front and bow shock construction will reveal that there are segments of wave fronts in front of the bow wave. This situation occurs just above the separating line between Region 2 and 3 of Fig. 1, and is seen in Figs. 2b and 3. Since each wave front represents a pressure signal, in this region the pressure starts to build up continuously just prior to the jump associated with the shock wave arrival.

As long as the sonic altitude ($a' = U$) is above the ground, parts of wave fronts will extend into the region ahead of the bow wave. We say "parts" for the following reason: At each point on the flight path disturbances propagate along rays in all directions. Those rays (Eq. (II.5)). which leave at angle $\epsilon_M = 90° - \mu$ carry the wave front segments which merge to form the envelope shock. There are also rays leaving at an angle $\epsilon_g > \epsilon_M$ (Fig. 3) which, due to refraction, become tangent to the ground and then bend upward. Any ray leaving at an angle greater than ϵ_g runs into the ground, we will consider the pressure signal ended there. Therefore sections of wave fronts corresponding to angles between ϵ_M and ϵ_g will continue propagating; it is just these sections which get in front of the bow wave.

If we draw a sequence of wave fronts and locate where the ray corresponding to ϵ_g meets each wave front we get the dashed line curve shown in Fig. 4. No direct signals from the aircraft can get ahead of this "signal cutoff" curve. Figure 4 is a scale drawing corresponding to a Mach 1.1 flight at 30,000 ft. Notice that the entire cutoff phenomenon is quite localized, within 1000 feet in the x direction and about 3,000 feet in the z direction.

Pressure transducers located at altitudes a, b, c, as shown in Fig. 4, would indicate readings shown in Fig. 5. Upstream of the "signal cutoff" curve and the bow wave there is no disturbance. At altitude a an ordinary "N" wave would be indicated by the transducer. In Fig. 5b the transducer would first see those acoustic pressure waves which arrive before the bow shock. Here the pressure builds up gradually until the shock arrives then there will be a pressure jump. Finally in Fig. 5c the transducer is in the subsonic region and its reading would be a continuous pressure buildup with no jumps.

II.3 THE WAVE FRONTS AS SUPERSONIC CHARACTERISTICS

As mentioned in the previous section the problem of a steady horizontal flight in an atmosphere which varies only in the vertical direction is time invariant. That is, the flow field surrounding the aircraft is always the same. Let us now consider the characteristic Eq. (II.1) for a steady two-dimensional flow:

$$u\,\phi_x + w\,\phi_z + a\,\sqrt{\phi_x^2 + \phi_z^2} = 0 \qquad \text{(II.12)}$$

On any surface $\phi(x, z) = \text{const}$

$$\phi_x = -\frac{dz}{dx}\,\phi_z \qquad \text{(II.13)}$$

Substituting (II.13) into (II.12) and solving for dz/dx

$$\frac{dz}{dx} = \frac{-uw \pm \sqrt{u^2 + w^2 - a^2}}{a^2 - u^2} \qquad \text{(II.14)}$$

which is the familiar (Ref. 8) expression for the characteristic slope in two-dimensional supersonic ($u^2 + w^2 > a^2$) flow.

This relation gives another clue as to the flow behavior in the sonic transition region and the subsonic to supersonic flow connection. In the subsonic region (Fig. 6) the wave fronts, all carrying pressure signals, propagate as in an ordinary subsonic flight. However these same wave fronts extend upward into the supersonic region where they correspond to ordinary supersonic characteristics. In fact, in the supersonic region they are somewhat like a Prandtl-Meyer type compression wave. (The analogy with the Prandtl-Meyer flow is for conceptual purposes only; one reason for a difference would be the nonuniform upstream flow).

In the compression region above the sonic line the flow is the same as that past a concave wall as shown, for example in Fig. 4.7 a, b on page 96, Ref. 9. Actually the bow shock outlined by the Prandtl-Meyer type compression is created by compression signals refracted from the subsonic region below. This is different from the bow wave at higher altitudes which is formed by compression signals directly from the aircraft. Since

the shock wave at its very end is slightly more than an enhanced characteristic it is quite weak and the boom strength is therefore small. The overall pressure increase, however, is caused by the shock plus the compression wave fronts upstream and downstream of it; therefore the total pressure rise can be somewhat greater than that across the shock

II.4 COMMENTS

The results given in the previous sections are based on wave front analyses. In regions where rays approach each other and form an envelope the ray tube theory of geometric acoustics is inapplicable. For our problem the free stream sonic line is an envelope, or caustic, of those rays leaving the aircraft at an angle $\epsilon = 90° - \mu$. (This result is classical and is discussed in several texts, e.g. Ref. 10 page 318, and Ref. 11 pages 141, 159). One of the requirements for application of geometric acoustics is that the flow field can have only slow variation along the ray. However we have seen that within a small domain about the cutoff region there are rather rapid changes in the pressure, for example. The major difficulty associated with a quantitative description of this problem is that the acoustic disturbances build up to change the flow field and the propagation properties. These changes in turn affect the disturbances, and it is this interplay of cause and effect which is so difficult to determine. The classical solutions to these problems in linearized optics are obtained by reverting to the wave front formulation as opposed to the ray tube formulation. This is just what we have done.

In Fig. 6 is a drawing of the flow field in the transonic interaction region. The sonic line for the true physical situation does not remain at a fixed altitude as it would for a linearized, acoustic solution. In addition streamlines are deflected upward and the shock, when it is formed within the compression region, probably bends slightly upstream.

CHAPTER III

THE REGION OF INCREASING SHOCK OVERPRESSURE

III.1 OBLIQUE SHOCK THEORY

It was mentioned at the end of Section II.3 that the shock, near its termination in the Prandtl-Meyer like region, can cause only a small pressure jump. We will show here that the region of increased overpressure occurs at the end of Region 1 of Fig. 1. Recall that the criterion for separating Regions 1 and 2 is that in 1 the flow behind the shock is supersonic while in 2 it is subsonic. We see then that in order to evaluate this criterion oblique shock relations are required.

Moeckel (Ref. 6) showed that as a shock propagates into a region of decreasing Mach number the pressure jump across the shock decreases and the shock angle (with the horizontal) increases. This behavior continues until the shock angle gets close to that angle at which subsonic flow occurs behind the shock, then the pressure jump starts to increase while the Mach number continues to decrease. Apparently the shock angle and Mach number vary in such a way as to cause the increasing pressure jump. Unfortunately, the method of analysis does not help explain this change in behavior, however an explanation based on physical reasoning is given in Section III.3. Lighthill (Ref. 7) states a similar finding but he does not give any details. Quoting from his paper: "The author attempted a more exact theory of the refraction of a shock entering a region of parallel and otherwise undisturbed steady flow at monotonically decreasing supersonic Mach number, which indicates that such an increase of strength occurs until a state is reached in which the flow behind the shock is subsonic; after this the refraction theory does not apply, but the shock presumably weakens".

The method developed below, which is essentially the same as Moeckel's, requires the flow behind the shock to be supersonic. Referring to Fig. 7, a shock is assumed to be propagating into a nonuniform region,

as it crosses each (horizontal) streamline a reflected Mach wave, separating Regions 3 and 4 of Fig. 7, is induced. We permit pressure variations across streamlines, such as would occur in the Earth's atmosphere, however we assume that the pressure ratio across the streamline remains constant:

$$\frac{p_2}{p_1} = \frac{p_4}{p_5} \tag{III.1}$$

Matching pressures in each section in Fig. 7:

$$\frac{p_5}{p_1} = \frac{p_5}{p_4} \cdot \frac{p_4}{p_3} \cdot \frac{p_3}{p_2} \cdot \frac{p_2}{p_1} = \frac{p_4}{p_3} \cdot \frac{p_3}{p_2} \tag{III.2}$$

where we have used Eq. (III.1).

Pressure ratios in Eq. (III.2) can be expressed in terms of Mach numbers and angles (M_2, θ_2) and (M_1, θ_1) by using Eqs. (128), (132), (139a), and the first two terms on the right hand side of (151) in Ref. 12. After making these substitutions let $M_1 = M_2 + \Delta M$ and $\theta_1 = \theta_2 + \Delta\theta$ and solve for $\Delta\theta/\Delta M$. The resulting expression is

$$\frac{\Delta\theta}{\Delta M} = \frac{-M(\sin^2\theta + A \cdot C)}{2M^2 \sin 2\theta + B \cdot C} \tag{III.3}$$

where

$$A = \left\{\sin 2\theta + \cot\theta\,(\gamma + \cos 2\theta)\right\} / D$$

$$B = \left\{(M^2 \cos 2\theta + \csc^2\theta)\left(1 + \frac{M^2}{2}(\gamma + \cos 2\theta)\right) + M^2 \sin 2\theta \left(\frac{M^2}{2}\sin 2\theta - \cot\theta\right)\right\} / D$$

$$C = (2\gamma M^2 \sin^2\theta - \gamma + 1)\, M_3^2 (M_3^2 - 1)^{-1}$$

$$D = \left\{1 + \frac{M^2}{2}(\gamma + 1 - 2\sin^2\theta)\right\}^2 + \left\{\frac{M^2}{2}\sin 2\theta - \cot\theta\right\}^2$$

$M, \theta = M_2, \theta_2$

M_3 is given in terms of M and θ in Eq. (132) of Ref. 12.

III. 2 A SAMPLE COMPUTATION

In order to compare different theories of shock strength near the cutoff altitude we have taken a sample flight, M = 1.1 at 40,000 ft. in a standard atmosphere and have computed shock overpressures using the computer program described in Ref. 13. For this flight condition the cutoff altitude is about 12,500 ft. At 20,000 ft. we determined M and θ to use as initial conditions for solving the differential Eq. (III. 3).

The results of this computation give the shock Mach number and inclination. From these, using oblique shock relations, we determined the pressure jump across the shock. However, these results (in fact this whole approach) are based on two-dimensional theory and are not corrected for the geometric axially symmetric spreading of the shock front. For a uniform atmosphere the above theory would predict a constant shock angle and Mach number. Actually since the shock is spreading away from its source it would weaken by $(\text{distance})^{-3/4}$ according to Whitham's theory, Ref. 2, Eq. (19). Therefore the pressure jump results obtained by integrating Eq. (III. 3) are "corrected" by including an attenuation proportional to $(\text{distance})^{-3/4}$. In Fig. 8 we compare pressure jumps obtained by the theory of Ref. 4 with those obtained by the present oblique shock approach. The numbers in parentheses are local pressure jumps; i.e., (pressure ratio, $\Delta p/p$X(local atmospheric pressure).

It is seen that the oblique shock theory, when carried to its limit of applicability, predicts pressure jumps about three times those of Ref. 4; however, we believe that an increase of order two times, as indicated at the bottom of page 8, would be more correct. This situation should be further discussed. First, the shock here is nearly vertical; for the above problem it was 87 degrees from horizontal. The ground reflection factor, therefore, should be near 1 instead of 2. Second, the theory is based on a mathematically perfect atmosphere. A slight variation in temperature could radically alter the whole picture; for example, a temperature increase of about 4 degrees would change the altitude of the pressure peak (in Fig. 8) from 13,700 to 15,000 feet. This sensitive dependence on local meteorological conditions is characteristic of shock behavior when its Mach number is very close to 1, say of order 1.005 as in the above problem; therefore, along or near the ground where temperatures vary

haphazardly, the only thing we can say is that the shock, if it exists at all, is very nearly vertical and reflection factors of 1 or even less are to be expected.

III. 3 COMMENTS

The theories of Refs. 2 and 4 do not use oblique shock relations. They consider a shock propagating down a ray tube with the shock front normal to the sides of the tube and hence use normal shock relations. For this approach the condition of the flow behind the shock; i. e., whether it is subsonic or supersonic, is disregarded. Whitham's original paper, Ref. 1, requires supersonic flow everywhere since that theory is based on properly locating the characteristics. And the ray tube theories, since they do not explicitly consider the shock angle, cannot completely describe some of the flow properties obtained by the oblique shock approach.

For the method described in this chapter, when the flow behind the shock approaches a Mach number of unity the reflected characteristics (Fig. 7) become nearly vertical. Since the incoming shock is also close to being vertical all the reflected pressure disturbances tend to remain in a vertical plane in the vicinity of the shock. Note, the pressure increase p_5/p_1 must match that across the shock p_3/p_2 plus that of the reflected wave p_4/p_3. Therefore there is a pressure buildup in this region. When the flow behind the shock is subsonic the pressure disturbances propagate away in all directions, hence this localized buildup cannot occur.

It seems that the ray tube approaches, Refs. 2 and 4, are valid when the flow behind the shock is either subsonic or supersonic, except for a region where the flow behind the shock approaches Mach 1. The regions of validity occur when the disturbances created by the shock are carried away by the flow behind the shock. In Ref. 6 Moeckel gets an analytic representation of the shock Mach number and angle at which the pressure stops decreasing and starts increasing with decreasing Mach number. However, this relation is rather involved and we have not been able to determine its physical significance, other than the reasoning given above.

The breakdown of ray tube theory is very similar to a situation described in Ref. 15. Here a shock propagating down a channel (or tube)

was considered; and a disturbance, such as a small change in tube area was introduced. When the flow behind the shock was either subsonic or supersonic a linear small disturbance theory was adequate for describing flow perturbations. However, when the shock strength was such that the flow behind was transonic the linear approach was inapplicable. It was shown that in this transonic case the pressure disturbances build up and sometimes coalesce to form a second shock.

CHAPTER IV

IMPROVEMENTS TO THE ACOUSTIC THEORY

IV.1 A PERTURBATION SOLUTION TO THE WAVE FRONT EQUATION

Because of the complicated nature of the flow in the cutoff region it is practically impossible to obtain an exact solution there. Furthermore, in light of the discussions given in the previous two chapters practically all of the flow properties are qualitatively known. Also, any attempted full flow field solution to the present idealized problem would probably be made worthless by adding some realistic parameters: wind variation, aircraft maneuvers and temperature inversions. We will therefore present in this chapter two techniques which improve the acoustic results of Chapter II.

The first technique starts with the partial differential Eq. (II.8) for the wave fronts. However, we will alter the sound speed definition:

$$\Phi_T - U\,\Phi_x + a^* \sqrt{\Phi_x^2 + \Phi_z^2} = 0 \qquad \text{(IV.1)}$$

The augmented sound speed is defined as follows:

$$a^* = a' (1 + \eta(s)) \qquad \text{(IV.2)}$$

Where s is distance along a ray and $\eta(s)$ is an increment added to the sound speed in order to better represent a true shock propagation speed. This increment is induced by a finite amplitude source as opposed to the point source used previously. For simplicity we will use Whitham's "far field" approximation, $\eta(s) \sim s^{-3/4}$. Referring to Eq. (3.12) of Ref. 4 and Eqs. (4.3) and (3.9) of Ref. 13:

$$a'(1+\eta) = a'\left(1 + \frac{\gamma+1}{4\gamma}\,\frac{\Delta p}{p}\right)$$

$$\therefore\ \eta = \frac{\gamma+1}{4\gamma}\,\frac{\Delta p}{p} = \frac{\gamma+1}{4\gamma}\,\frac{K}{s^{3/4}} \qquad \text{(IV.3)}$$

where $K = \dfrac{M^{3/4} \cdot L^{3/4} \cdot VF}{(M^2-1)^{1/4} \cdot FR}$

M = aircraft Mach number

L = aircraft length

VF = volume factor

FR = fineness ratio

We will obtain a perturbation solution to Eq. (IV.1) of the form

$$\Phi(T, x, z) = \phi(T, x, z) + \psi(T, z) \tag{IV.4}$$

where $\phi = x + U\lambda - \dfrac{a}{k}\sqrt{\dfrac{2a'}{a}\cosh k\lambda - \left(\dfrac{a'}{a}\right)^2 - 1}$

$\lambda = T - \tau$, $a' = a - k(z-h)$

The function ϕ is the acoustic wave front, given in Eq. (II.6). If we equate Φ to zero we see that the perturbation term ψ is an increment added to the x coordinate of the acoustic solution. We relate ψ to the sound speed perturbation, η, by substituting (IV.4) into Eq. (IV.1), retaining first order terms

$$\psi_T + \frac{a'(\cosh k\lambda - \frac{a'}{a})}{\sinh k\lambda}\psi_z + \frac{a'\eta \sinh k\lambda}{\sqrt{\frac{2a'}{a}\cosh k\lambda - (\frac{a'}{a})^2 - 1}} = 0 \tag{IV.5}$$

The characteristic equations for Eq. (IV.5) are

$$\frac{dz}{dT} = \frac{a'(\cosh k\lambda - \frac{a'}{a})}{\sinh k\lambda} \tag{IV.6}$$

$$\frac{d\psi}{dT} = -\frac{a'\eta \sinh k\lambda}{\sqrt{\frac{2a'}{a}\cosh k\lambda - (\frac{a'}{a})^2 - 1}} \tag{IV.7}$$

Equation (IV.6) is the same as the characteristic equation that would be found from the original acoustic Eq. (II.8); it is, in fact, the equation for the ray locus. This can be seen by eliminating λ, using

Eq. (II.11); the resulting differential equation is the same as the one corresponding to Eq. (4) of Ref. 3.

The solution to Eq. (IV.7) can be written formally by integrating with respect to T. Since the characteristic curves, given by Eq. (IV.6), are rays, the integration is along a ray:

$$\psi = - \int_{\tau}^{T} \frac{a' \eta \sinh k\lambda \, dT'}{\sqrt{\frac{2a'}{a} \cosh k\lambda - (\frac{a'}{a})^2 - 1}}$$

The above integral can be considerably simplified by substituting $\lambda' = T' - \tau$ and eliminating a' by means of Eq. (II.11):

$$\psi = - a \sec \epsilon \int_{0}^{\lambda} \eta(s) \, d\lambda' \qquad \text{(IV.8)}$$

Therefore the improved wave front equation is

$$\Phi(T, x, z) = 0$$

$$\text{or} \quad x = - U\lambda + \frac{a}{k} \sqrt{\frac{2a'}{a} \cosh k\lambda - (\frac{a'}{a})^2 - 1} + a \sec \epsilon \int_{0}^{\lambda} \eta(s) \, d\lambda' \qquad \text{(IV.9)}$$

In the integral term of Eq. (IV.9) distance, s, can be found by integrating

$$ds = dx \sqrt{1 + (\frac{dz}{dx})^2}$$

along the ray, using Eq. (II.5) to determine $\frac{dz}{dx}$. After carrying out this integration x and z can be eliminated in terms of ϵ and λ using Eqs. (II.5) and (II.11). The resulting expression is

$$s = \frac{a \sec \epsilon}{k} \left\{ \epsilon + \sin^{-1} \left[\frac{\tanh k\lambda - \sin \epsilon}{1 - \sin \epsilon \tanh k\lambda} \right] \right\} \qquad \text{(IV.10)}$$

By fixing a value of the time parameter λ a specific wave front is identified by Eq. (IV.9). There is one difficulty, however, due to the fact that the correction term involves an integration along a ray and each point on the wave front corresponds to a different ray. The x, z coordinates for any wave front, λ, can be determined as follows: For any altitutde z Eq. (II.11) can be used to determine the corresponding ϵ, this identifies the ray. With ϵ known we can use Eq. (IV.10) in (IV.9) to solve for the x coordinate on the wave front.

The bow shock front is determined by finding the envelope of the improved wave fronts, Eq. (IV.9). A parametric representation, like Eq. (II.9), between z and λ along the envelope is obtained by taking the partial derivative of Eq. (IV.9) with respect to λ:

$$\cosh k\lambda = \frac{(U - U\eta)^2}{aa'} \pm \sqrt{\left[\left(\frac{U - U\eta}{a}\right)^2 - 1\right]\left[\left(\frac{U - U\eta}{a'}\right)^2 - 1\right]} \qquad \text{(IV.11)}$$

In determining (IV.11) the angle ϵ was eliminated by setting $\cos \epsilon = a/U = 1/M$. This relation, in accordance with the discussion leading to Eq. (II.11), implies that those rays, carrying wave front segments which form the envelope or shock, leave the aircraft at angle $\epsilon = 90° - \mu$, where μ is the Mach angle. The cutoff altitude for the improved shock front is found from the vanishing of the square root in Eq. (IV.11); that is, when

$$U = \frac{a'}{1 - \eta} \cong a'(1 + \eta)$$

We see, then, that the cutoff altitude occurs when the "improved" propagation speed equals the aircraft speed. This differs from the acoustic theory of Chapter II, there the cutoff altitude was where the local atmospheric sound speed equals the aircraft speed. The above definition for the cutoff altitude is in agreement with Ref. 4 Eq. (3.8) where it was shown that the shock front became vertical (which, for the present problem, is equivalent to cutoff) at that altitude where the shock velocity equals the aircraft speed.

It is not difficult to estimate what effect the improvement "η" will have on the acoustic solution, given in Eqs. (II.5) and (II.6). First, the x coordinate of the shock is lengthened by

$$a \sec \epsilon \int_0^{\lambda} \eta(s)d\lambda \sim a \sec \epsilon \cdot \eta_{av} \lambda \sim 1000 \cdot 10^{-3} \cdot 100$$

$$= 100 \text{ ft.}$$

That is the x coordinate of the shock will be about 100 ft. upstream of the acoustic wave front envelope. To get this estimate we used $\eta \sim 10^{-3}$ since it is of order $\Delta p/p$ (see Eq. IV.31); also the travel time λ is about 100 sec., and $\sec \epsilon \sim 1$.

The change in the z coordinate can be estimated from the cut-off relation given in the previous paragraph:

$$a' = a + k(z-h) = U(1-\eta)$$

Let $a = 1000$ ft./sec., $U = 1100$ ft./sec., $k = .004$ sec.$^{-1}$,

$h = 30{,}000$ ft., $\eta = 10^{-3}$

acoustic cutoff $z = h + \dfrac{a-u}{k} = 5{,}000$ ft.

improved cutoff $z = h + \dfrac{a-u}{k} + \dfrac{u\eta}{k} = 5{,}250$ ft.

That is the cutoff altitude is about 250 ft. higher with the improved approximation.

IV.2 AN IMPROVED WAVE FRONT DETERMINATION*

The technique described here permits a more accurate estimate of the shock shape while using the acoustic results obtained in Chapter II. We know that the disturbance propagating from the aircraft travels at a speed greater than the free stream sound speed (see, for example, Eq. 4 of Ref. 2). Therefore the basic idea behind this approach is to prescribe a sound speed, varying linearly with altitude, but which permits a more exact description of the true propagation speed. Since we will keep the linear sound speed variation, all the wave front and ray equations used in Chapter II can be retained.

The "sound speed", A, used here is (see Eq. (II.7) for comparison).

$$A = \alpha - \beta (z - h) \tag{IV.12}$$

where h is aircraft altitude, and the two parameters α and β are to be determined. First, α is determined by having the slope of the wave front envelope equal the slope of the bow wave at the aircraft. The bow wave slope, $\tan \theta_h$, is known in terms of the aircraft Mach number and nose angle. At its origin ($z = h$, $x = \lambda = 0$ in Eqs. (II.6) and (II.10)) the wave front envelope slope is, in terms of α instead of a,

$$\frac{dz}{dx} = \frac{\alpha}{\sqrt{U^2 - \alpha^2}} \tag{IV.13}$$

Equating the bow wave and the envelope slopes

$$\frac{\alpha}{\sqrt{U^2 - \alpha^2}} = \tan \theta_h$$

or

$$\alpha = U \sin \theta_h \tag{IV.14}$$

(If the bow wave is detached neither this nor any of the "uniformly valid" solutions are applicable near the aircraft. In this case the shock slope would have to be matched at some distance from the aircraft, where Whitham's theory is applicable).

---

* This method of improving upon acoustic theory results was developed by David C. Chou, a graduate student at MIT.

At the ground we are far from the aircraft and well into the subsonic region of Fig. 1. We therefore assume that the wave front propagation speed here is equal to sound speed. Therefore the parameter β is found by setting $A = a_g$ at $z = 0$:

$$A = \alpha + \beta h = a_g$$

$$\text{or} \qquad \beta = \frac{a_g - \alpha}{h} = \frac{a_g - U \sin \theta}{h} \qquad \text{(IV.15)}$$

where a_g = sound speed at the ground.

We are now able to use all the equations given in Chapter II after making the following substitutions:

substitute A for a'

α for a

β for k

IV.3 NUMERICAL RESULTS

Since the approach described in Section IV.2 is easy to evaluate we carried out a computation for a Mach 1.1 aircraft flying at 30,000 ft. (In order to have an attached shock a nose angle of 1° was assumed). The results are given in Fig. 9. Also given in Fig. 9 are results for the same flight conditions as computed by acoustic theory (Eqs. (II.5), (II.6)), and by the Sonic Boom Computer Program described in Ref. 13. The latter results are given by heavy dots.

We see that the SBCP data agrees, for the most part, with the acoustic results. The theory of Section IV.2 predicts perturbation effects which are too large. From estimates derived at the end of Section IV.1 the difference between improved and acoustic theories should be of order 200 ft. in cutoff coordinates. The theory of Section IV.2 predicts differences of order 1500 ft.

CHAPTER V

SUMMARY

V.1 A REVIEW OF THE FINDINGS

The results of the previous sections enable us to describe the shock wave behavior in the neighborhood of the sonic cutoff altitude. We have not given a solution to a specific problem. (Although we did use a special atmospheric temperature model, it is felt that this model is realistic and the results are quite general.) Rather, we have presented a considerable amount of evidence based on the theory of characteristics, acoustical theory, and oblique shock theory. By using and combining these theories we have been able to present a logical description of the various physical phenomena in the shock cutoff region.

To review the findings, we see that the shock at first propagates away from the aircraft in a manner like that described in Refs. 1, 2, 4. That is, the pressure jump across the shock decreases as it moves outward. Because (as we have assumed) the sound speed increases as the ground is approached, the shock Mach number decreases. In addition, due to refractive effects, the shock inclination to the horizontal approaches 90°. As the shock continues moving into the higher temperature region its Mach number and inclination combine so as to cause the flow behind the shock to become subsonic, this being determined by oblique shock theory. None of the above references adequately describe the flow behavior as this subsonic (behind the shock) region is approached. It was shown in Chapter III that although the shock Mach number is decreasing, its inclination combines with the Mach number so as to cause the pressure jump across the shock to increase. This increase, as discussed in Section III.3, is caused by the tendency of reflected disturbances to remain in the vicinity of the shock. Instead of propagating away, downstream, they build up inducing overpressures of order twice those predicted by Ref. 4.

As we continue down the shock front, into the region where the flow behind the shock is subsonic, the overpressures start decreasing again since the disturbances behind the shock are again able to propagate away. This is borne out in Ref. 14 where an experiment was described in which a shock was propagated down a tube which had a heated base plate. This heating induced a vertical temperature gradient parallel to the shock front, which had only subsonic flow behind it. For cases in which the shock reached the base plate the pressure jump across the shock decreased as vertical distance above the plate decreased. That is the pressure jump was smaller in the hotter regions.

Continuing further down the shock front we get to a region where compression wave fronts have arrived ahead of the shock. These fronts are signals traveling along rays which have entered regions where the propagation speed is greater than the aircraft speed. There is a definite limited region, set by the ground the temperature profile and the aircraft altitude and Mach number, in front of the shock where these signals can reach. The flow configuration, such as indicated in Fig. 6, is a steady one, moving with the shock at aircraft speed. The compression wave fronts, being characteristic surfaces, form a Prandtl-Meyer like compression fan and the shock ends embedded in this fan. Actually it would be more accurate to say that the shock is formed here, by the compression signals rising from the subsonic region below.

This description is again in agreement with the results of Ref. 14, when the base plate in the shock tube was heated enough that sound speed near the plate was greater than the shock speed. A steady configuration was attained in which the shock vanished, somewhere above the sonic altitude, embedded in a compression region which extended upstream of the main shock front (see Fig. 10 of Ref. 14).

It is believed that the pressure increase across the region of the combined shock plus compression wave fronts remains fairly constant. However the pressure jump across the shock alone decreases until it vanished completely, from this point down the pressure increase is smooth with no jumps.

Below this region, where the flow is completely subsonic, the pressure increase is like that below a subsonic aircraft. There is however,

one major difference. For a steady subsonic flow the pressure signals theoretically reach infinitely far upstream. In the present problem the signals are confined behind a "signal cutoff" curve. All this, of course, neglects reflections off the ground and propagation through the ground.

V.2 LATERAL CUTOFF

All the previous discussions considered only the vertical (x, z) plane containing the aircraft flight path. We will now show that the flow behavior on either side of the (x, z) plane is essentially the same as that already described. The physics of the situation is unchanged and all that is altered is the geometry.

Let us first recall the fact, proven in the Appendix of Ref. 4, that (in the absence of winds) any ray will always remain in its initial vertical plane. Furthermore the refractive properties of this ray are set by the component of the aircraft velocity in this plane.

In order to demonstrate the latter fact consider Eq. (II.11) which relates propagation time and altitude for any ray leaving at an initial angle ϵ. Also consider Eqs. (II.9) and (II.10) which refer to rays in the x, z plane leaving at angle $\epsilon = 90° - \mu$; rays which leave at this angle carry wave front segments which form the bow shock. Let us now generalize the angle ϵ to mean the angle between any shock forming ray and the horizontal plane. For a vertical plane making an angle ω with the x, z plane it is shown in Fig. 10 that

$$\cos \epsilon \cdot \cos \omega = a/U$$

$$\text{or} \qquad \cos \epsilon = a/U \cos \omega \qquad \text{(V.1)}$$

For the vertical (x, z) plane through the flight path $\omega = 0$ and $\cos \epsilon = a/U$. Therefore for any angle ω the only change in Eqs. (II.9) and (II.10) is to write U cos ω instead of U:

$$\cosh k\lambda = \frac{U^2 \cos^2 \omega}{a a'} \pm \sqrt{\left\{\left(\frac{U \cos \omega}{a}\right)^2 - 1\right\}\left\{\left(\frac{U \cos \omega}{a'}\right)^2 - 1\right\}}$$

$$a' = a \left\{\cosh k\lambda - \sqrt{1 - \left(\frac{a}{U \cos \omega}\right)^2} \sinh k\lambda\right\}^{-1} \qquad (V.2)$$

We see then that, as stated previously, the refractive properties of the ray and the shock front are fixed by the component of the aircraft velocity in the ω plane. Therefore for this case lateral cutoff occurs sooner in time and at a higher altitude than under the aircraft.

Another way to look at the result (V.2) is as follows: Any wave front, and hence the shock, always propagates in a direction normal to its surface (see Eq. (II.4)); also since the rays are normal to the surface, the front always propagate in the same lateral plane defined by angle ω. Therefore the wave front in any lateral plane sees a free stream flow of magnitude $U \cos \omega$. Hence starting at the "Mach angle" $\sin^{-1}\left(\frac{a}{U \cos \omega}\right)$ the lateral shock propagates through the same type of regions and exhibits the same sort of phenomena as the shock below the aircraft, already described.

REFERENCES

1. Whitham, G.B., "The Flow Pattern of a Supersonic Projectile", Amm. Pure and Appl. Math., Vol. V, p. 301, 1952.

2. Whitham, G.B., "On the Propagation of Weak Shock Waves", J. Fl. Mech., Vol. I, p. 290, 1956.

3. Lansing, D.L., "Application of Acoustic Theory to Predictions of Sonic-Boom Ground Patterns from Maneuvering Aircraft", NASA TN D-1860, October 1964.

4. Friedman, M.P., Kane, E.J. and Sigalla, A., "Effects of Atmosphere and Aircraft Motion on the Location and Intensity of a Sonic Boom", AIAA J., Vol.I, No. 6, p. 1327, 1963.

5. Randall, D.G., "Methods for Estimating Distributions and Intensities of Sonic Bangs", British Aero. Research Council R and M No. 3113, 1959.

6. Moeckel, W.E., "Interaction of Oblique Shock Waves with Regions of Variable Pressure, Entropy, and Energy", NACA TN 2725, June 1952.

7. Lighthill, M.J., "Reflection at a Laminar Boundary Layer of a Weak Steady Disturbance to a Supersonic Stream, Neglecting Viscosity and Heat Conduction", Q.J.M.A.M., Vol. III, pt. 3, p. 303, 1950.

8. Ferri, A., General Theory of High Speed Aerodynamics, Vol. VI, p. 589, Ed. W.R. Sears, Princeton Univ. Press, 1954.

9. Liepmann, H.W., Roshko, A., Elements of Gasdynamics, Fig. 4.7a, b, p. 96, Wiley and Son, 1957.

10. Summerfield, A., Optics, Academic Press, 1954.

11. Landau, L.D., Lifshitz, E.M., The Classical Theory of Fields, Addison Wesley, 1959.

12. Ames Research Staff, "Equations, Tables and Charts for Compressible Flow", NACA Rpt. 1135, 1953.

REFERENCES (Continued)

13. Friedman, M. P., "A Study of Atmospheric Effects on Sonic Booms", MIT Aerophysics Laboratory, Technical Report 89, April 1964.

14. Griffith, W. C., "Interaction of a Shock Wave with a Thermal Boundary Layer", J. Aero. Sci., Vol. 23, p. 16, 1956.

15. Friedman, M. P., "An Improved Perturbation Theory for Shock Waves Propagating through Nonuniform Regions", J. Fl. Mech. Vol. 8, p. 193, 1960.

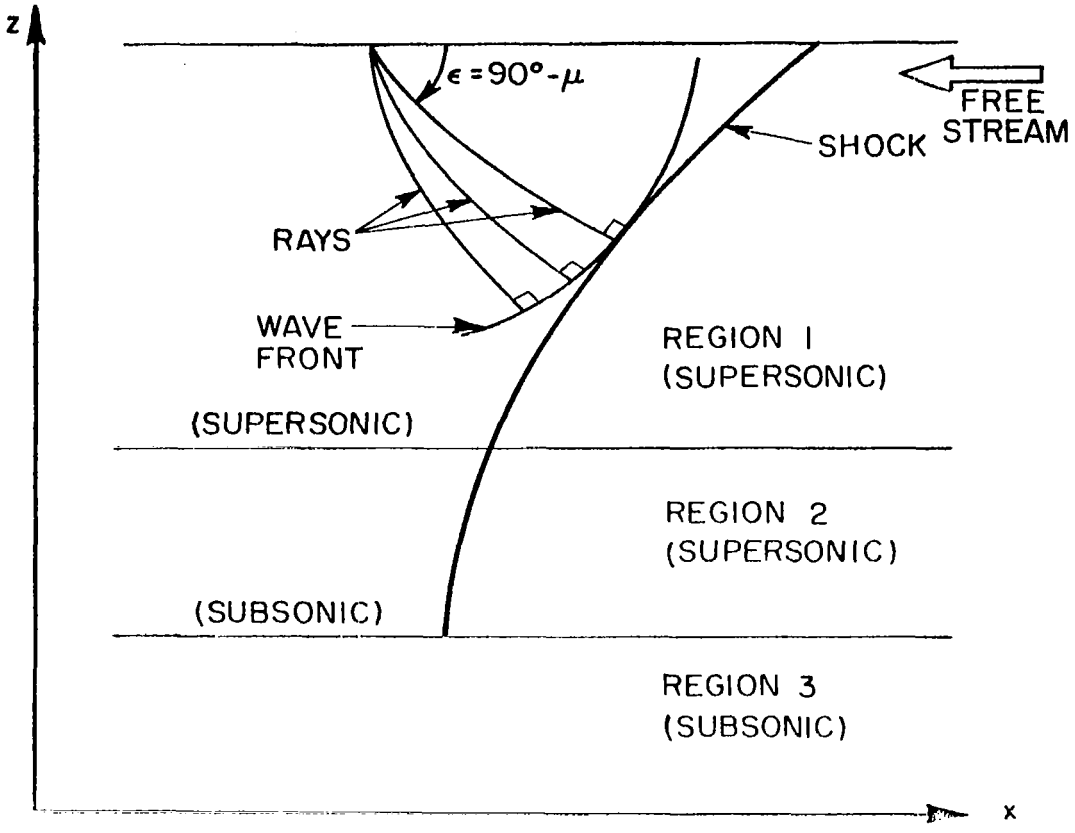

Figure 1. Flow regions between aircraft and ground

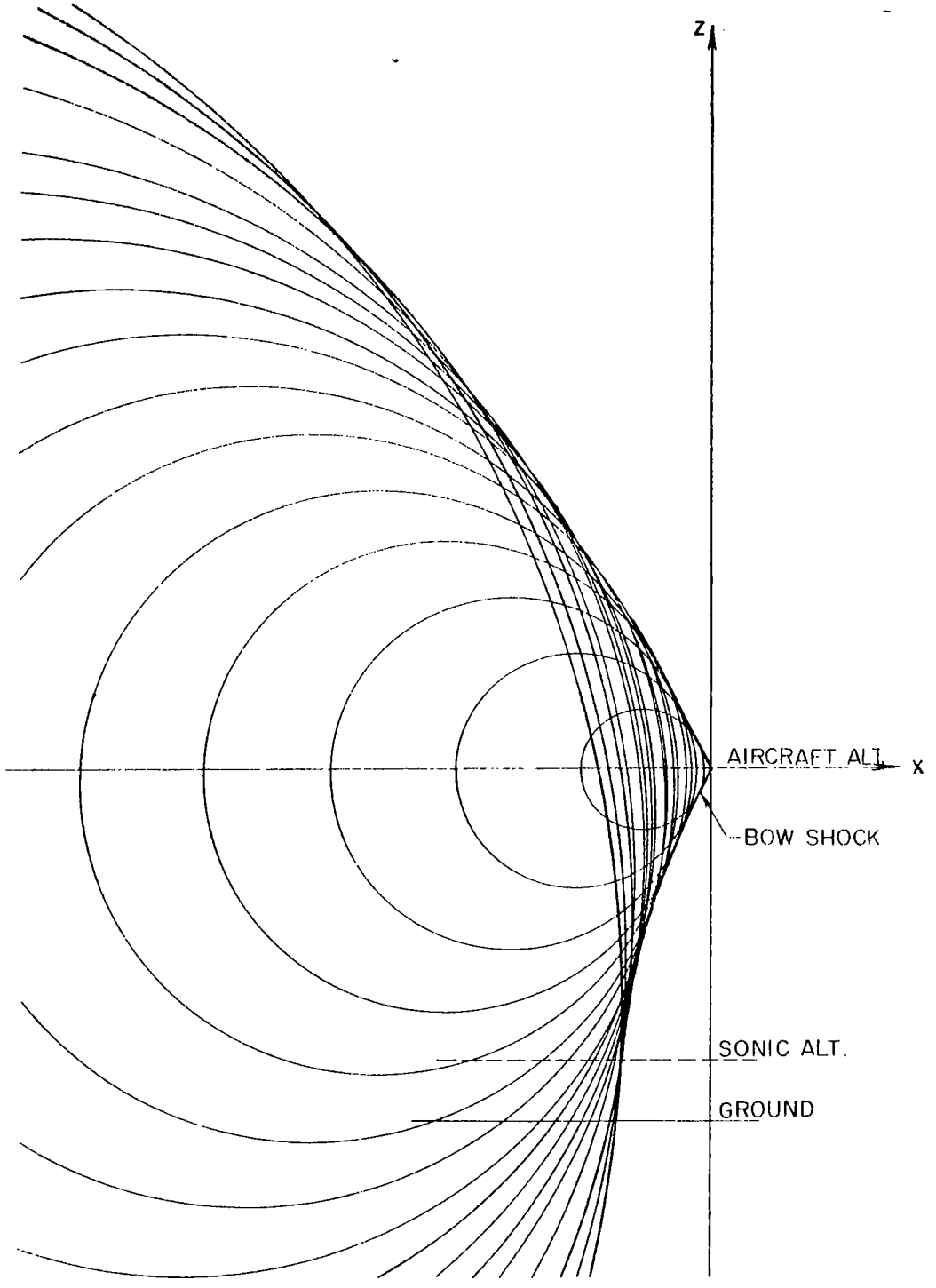

Figure 2a. Wave front construction of bow shock

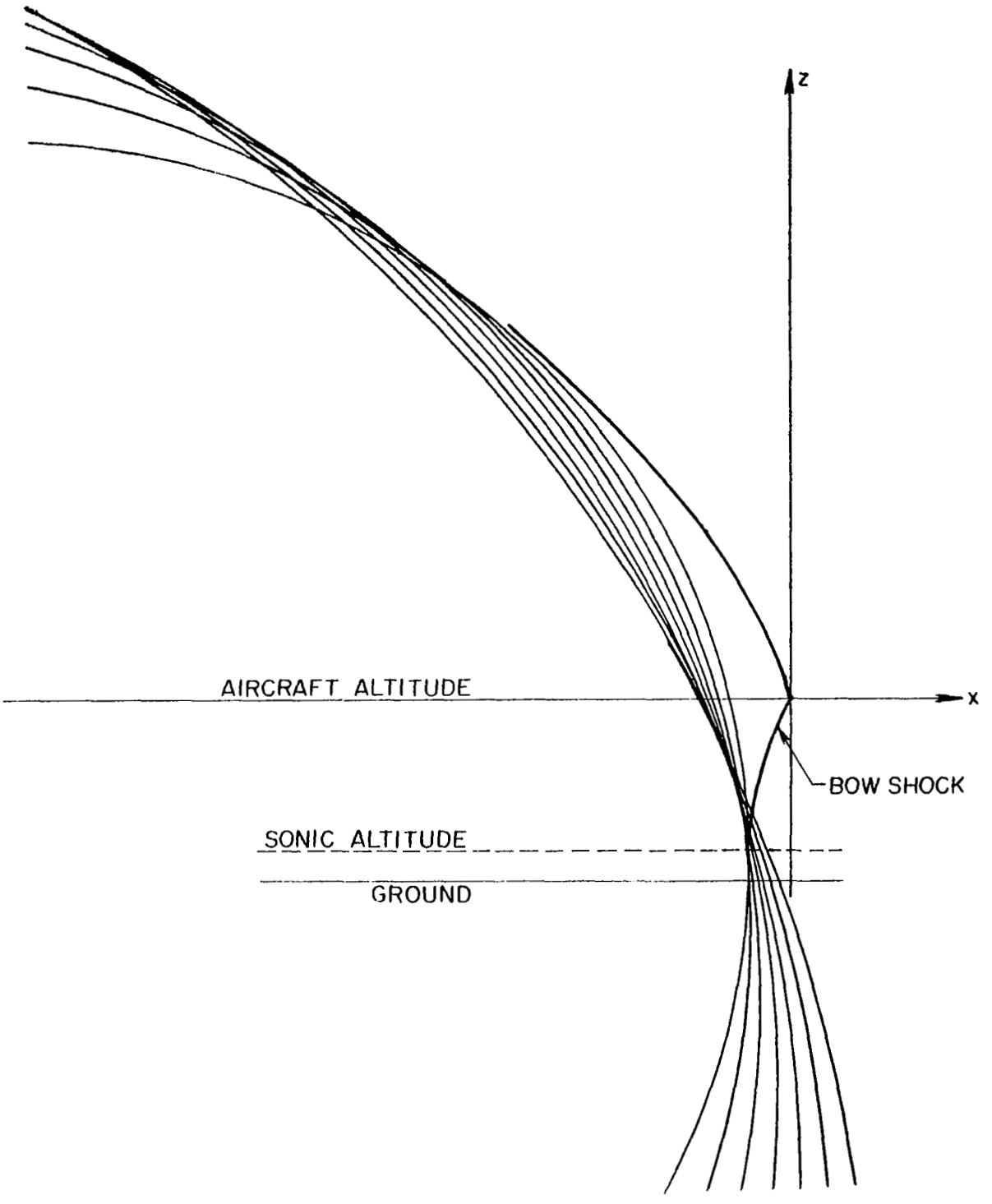

Figure 2b. Wave front construction of reflected shock

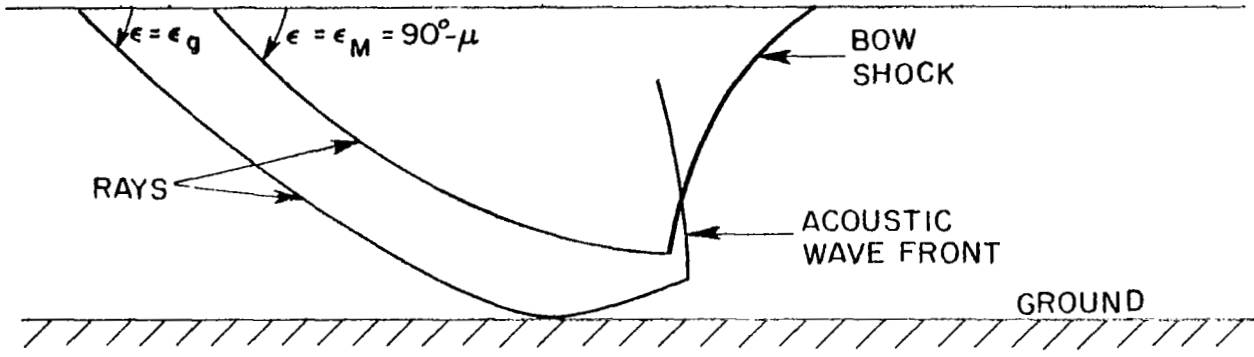

Figure 3. Locus of ray tangent to the ground and a wave front ahead of the bow shock

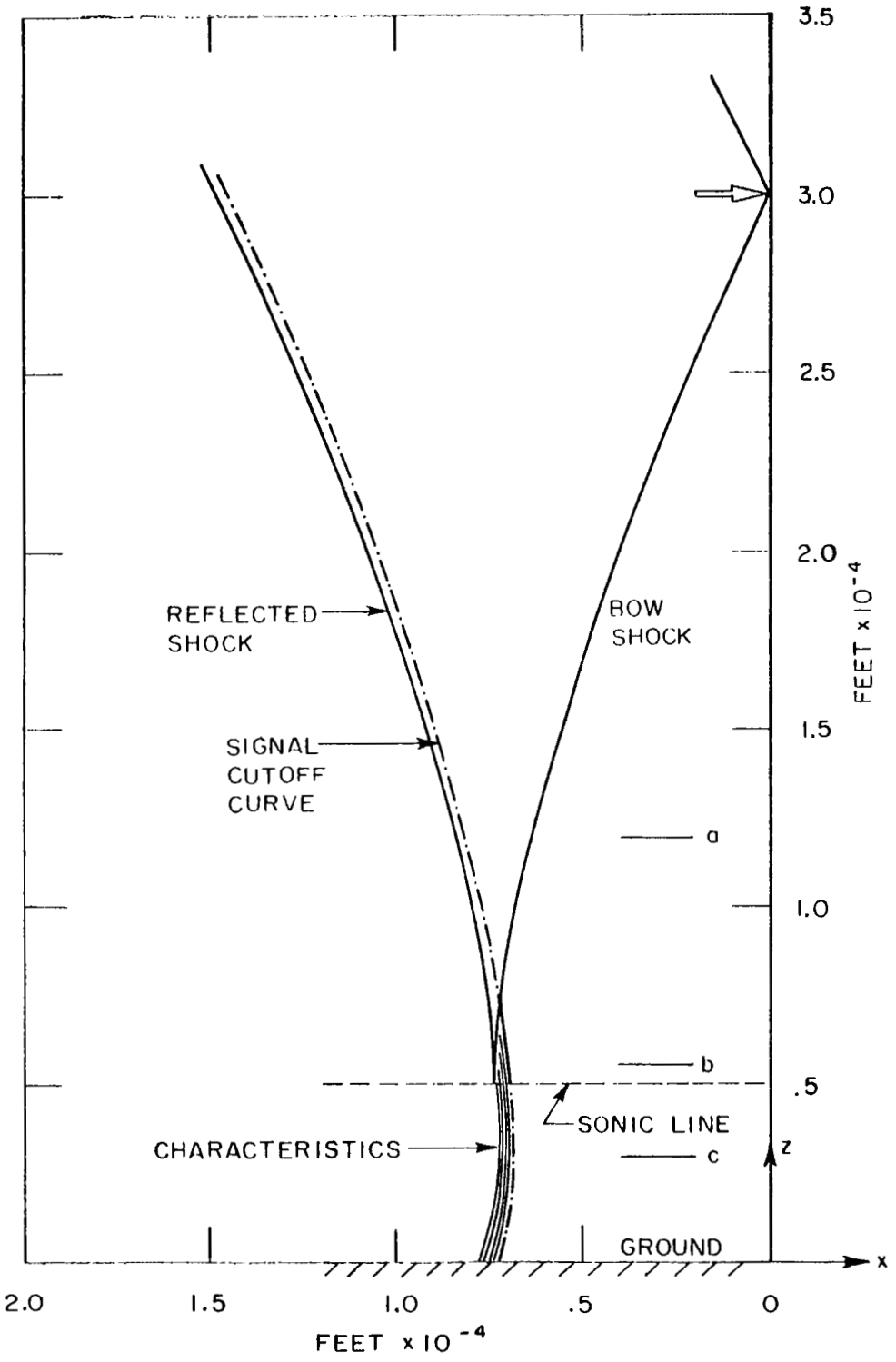

Figure 4. Location of the signal cutoff curve, bow and reflected shock for a M = 1.1 flight at 30, 000 ft.

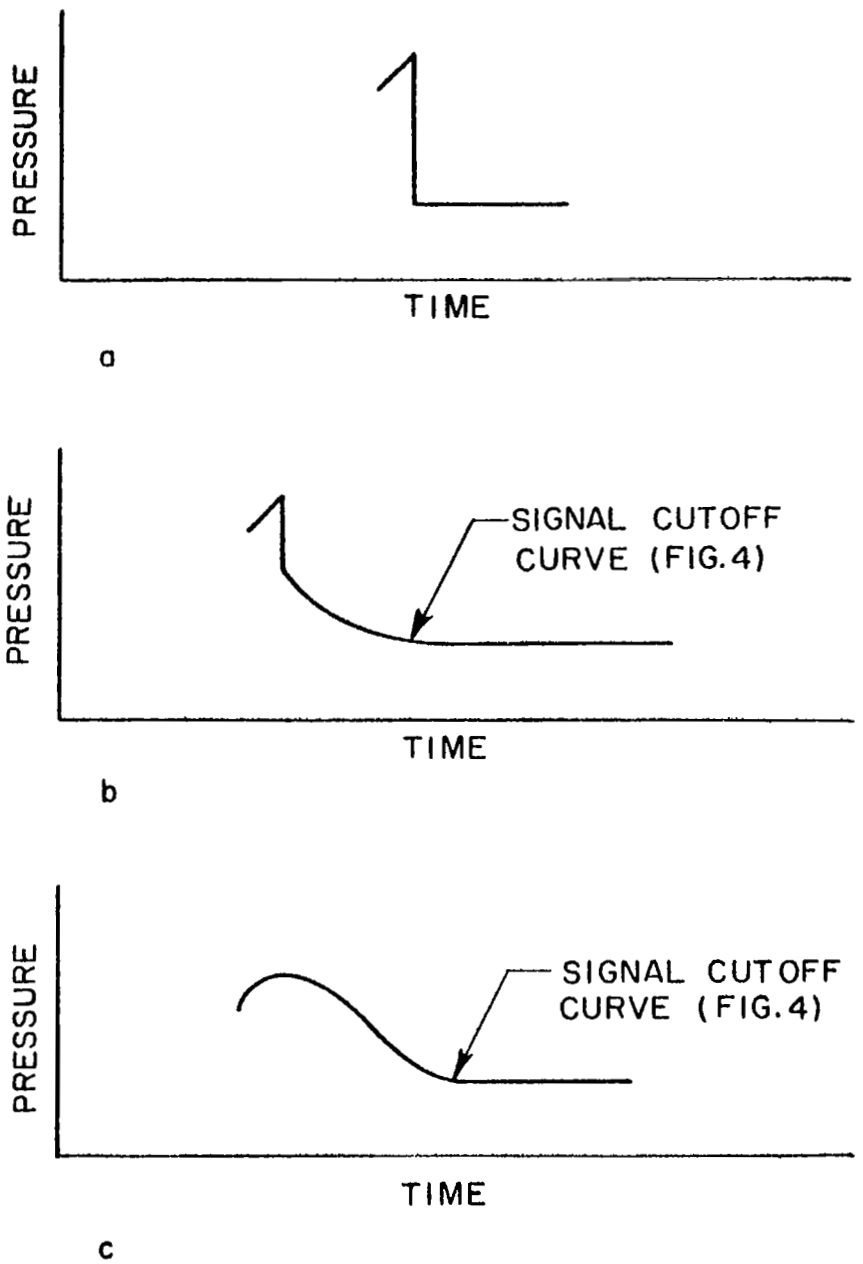

Figure 5. Pressure transducer readings at altitudes a, b, c in Fig. 4

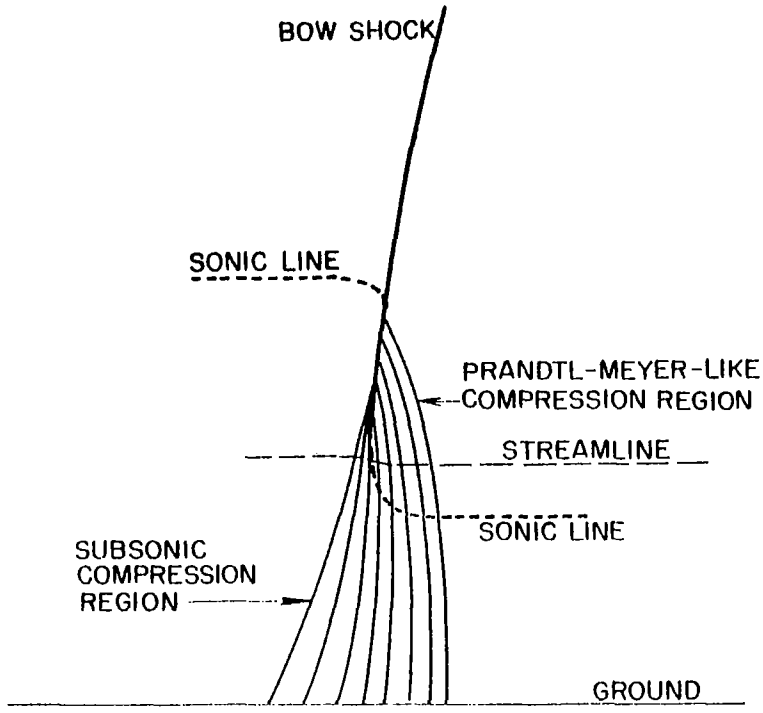

Figure 6. A detail of the flow field near the cutoff altitude

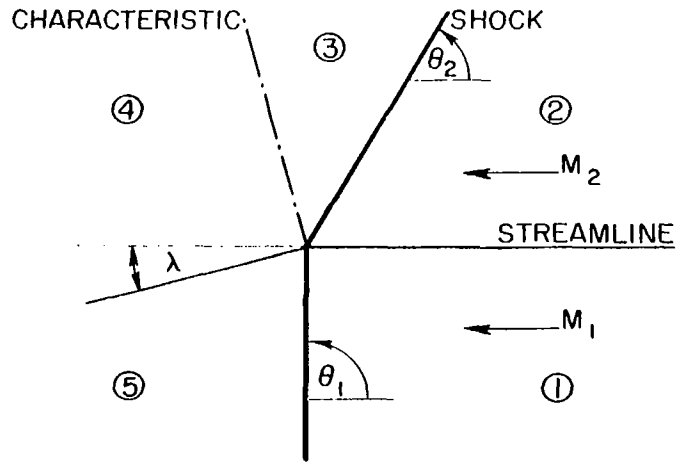

Figure 7. Shock wave interacting with a nonuniform region

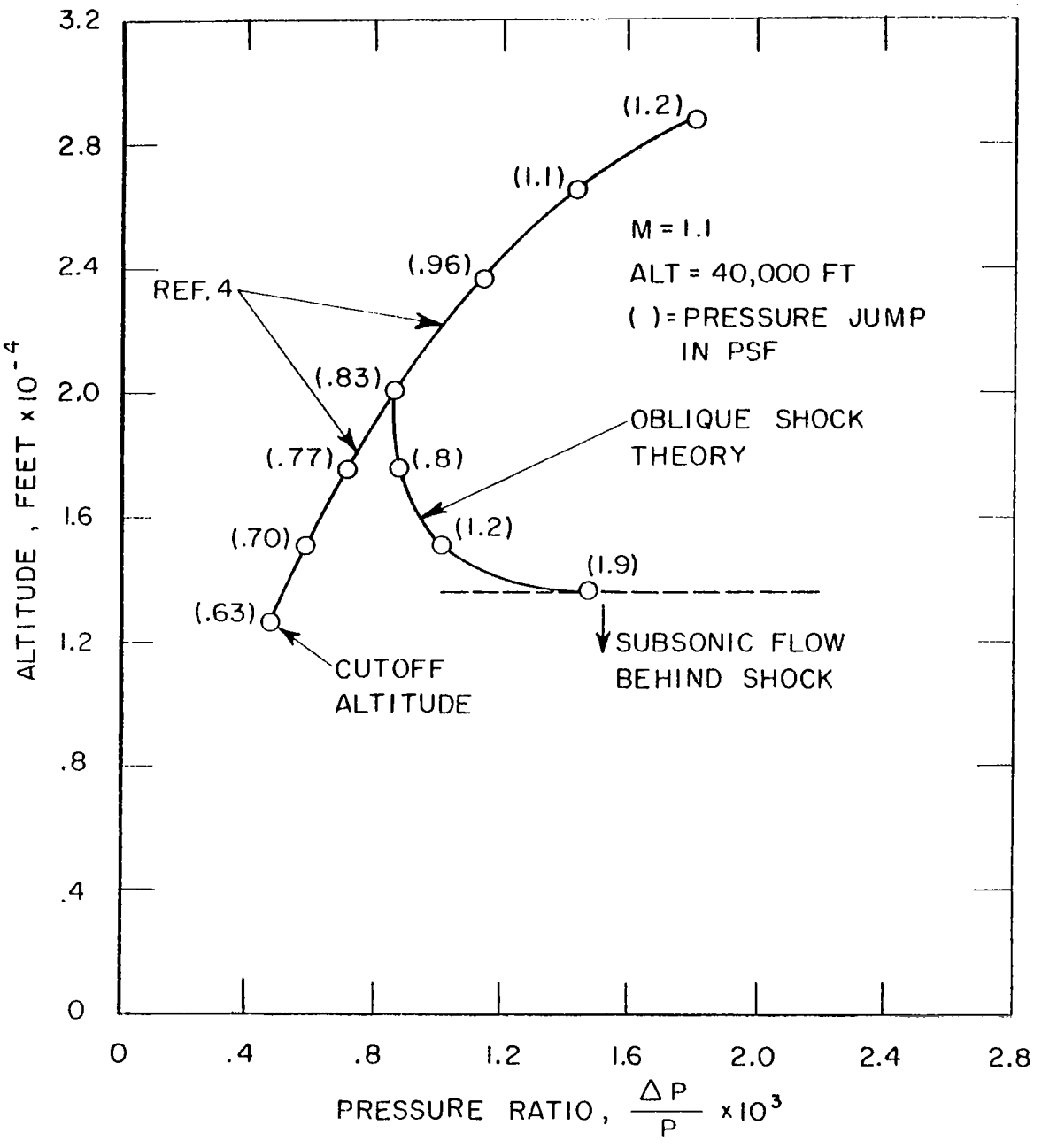

Figure 8. A comparison of overpressures predicted by the oblique shock theory of Section III.1 and the theory of Ref. 4

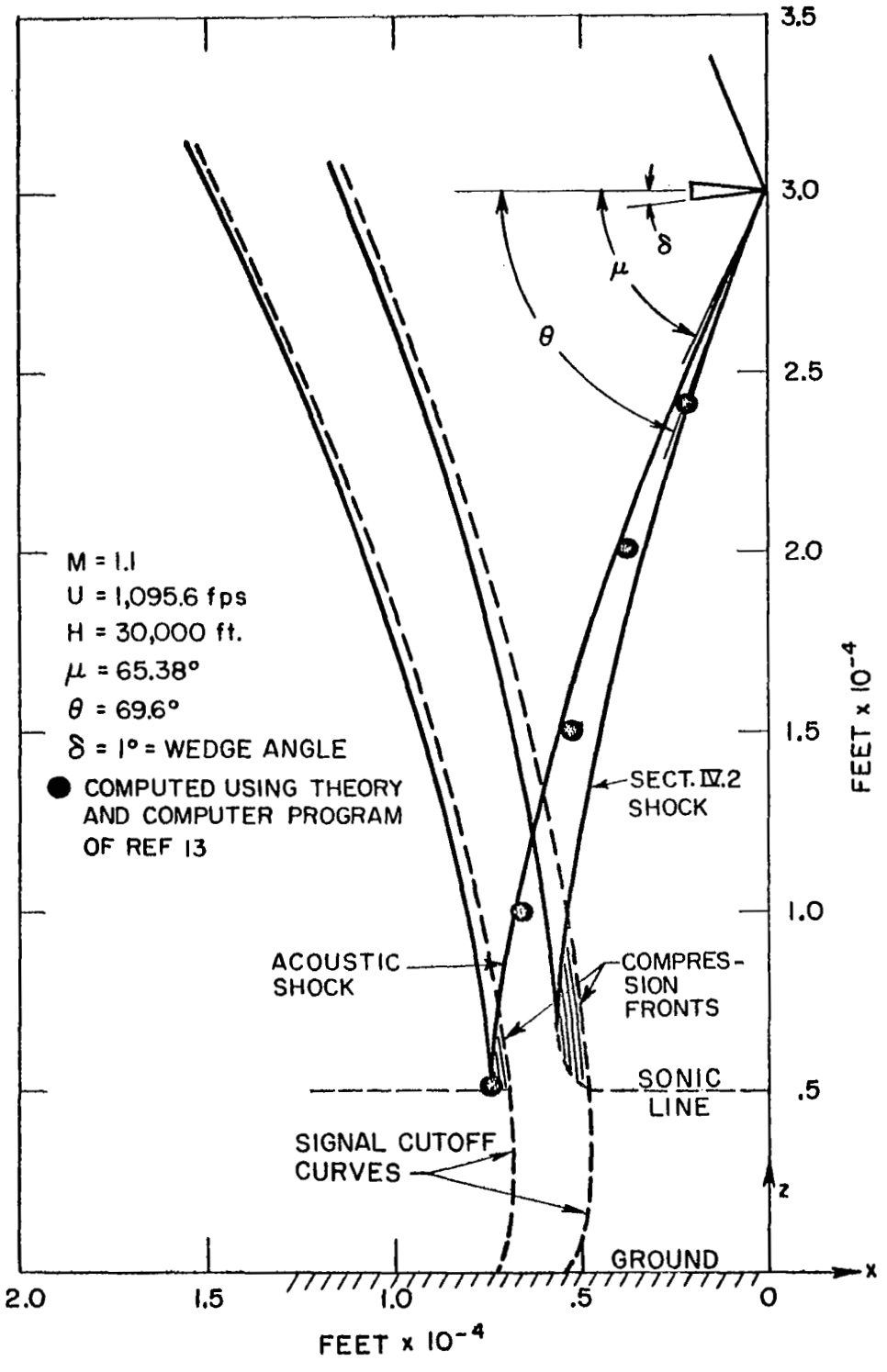

Figure 9. A comparison of different methods for locating the shock front

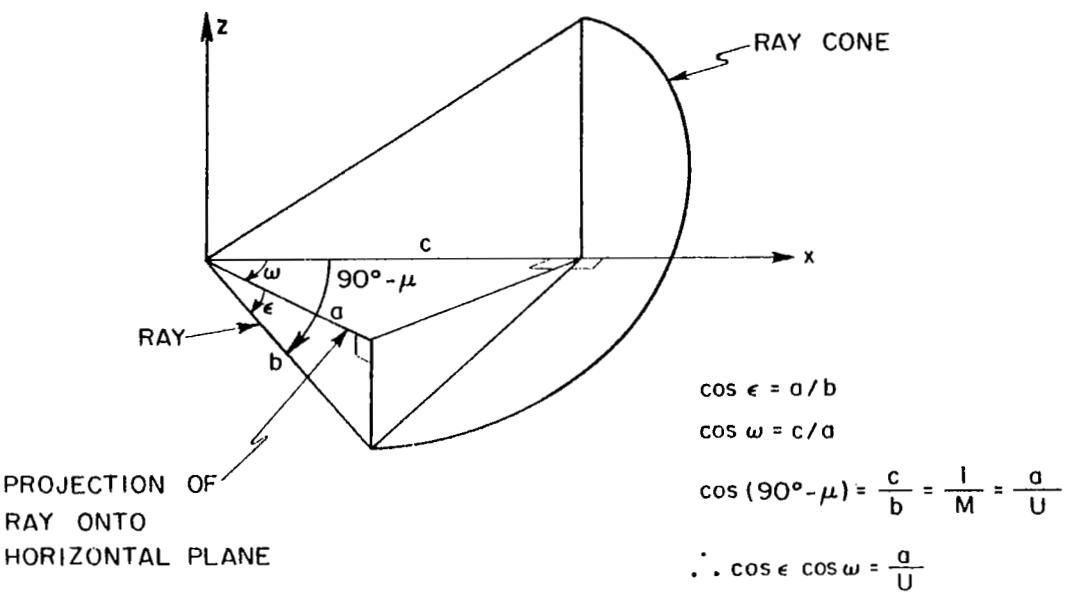

Figure 10. Ray cone geometry for determining ray angles for lateral propagation

APPENDIX A

DERIVATION OF CHARACTERISTIC EQUATION

For completeness, the equations of characteristic surfaces for the Eulerian flow equations will be derived here. These equations are (using the convention of summing on repeated subscripts):

$$\rho_t + (\rho u_i)_{x_i} = 0$$

$$u_{i_t} + u_j u_{i_{x_j}} + \frac{1}{\rho} p_{x_i} = 0 \qquad \text{(A-1)}$$

$$p_t + u_i p_{x_i} - \frac{\gamma p}{\rho} (\rho_t + u_i \rho_{x_i}) = 0;\ i, j = 1, 2, 3$$

A characteristic surface $\phi(t, x_i)$, for any partial differential equation, has the property that if data are prescribed on the surface $(\rho(\phi),\ p(\phi),\ u_i(\phi))$ then the partial differential equation cannot be used to find values of (ρ, p, u_i) outside of ϕ. That is the outward derivative, from ϕ, cannot be found and the data cannot be extended from the initial surface. The given partial differential equation, for such a situation, is essentially a tangential derivative on the surface.

The direction cosines, ξ_k, for the normal to the surface $\phi(t, x_i)$ are defined as follows:

$$\left(\frac{\phi_t}{Q}, \frac{\phi_{x_i}}{Q}\right) = (\xi_0, \xi_i) \equiv (\xi_k) \qquad \text{(A-2)}$$

where $Q = \sqrt{\phi_t^2 + \phi_{x_i}^2}$; $i = 1, 2, 3$; $k = 0, 1, 2, 3$

The normal derivatiove from the surface ϕ is

$$\frac{d}{dn} = \xi_k \frac{\partial}{\partial x_k}, \text{ where } x_0 = t \qquad \text{(A-3)}$$

Any directional derivative, $a_k \frac{\partial}{\partial x_k}$, is a tangential derivative on ϕ if $\xi_k a_k = 0$; also, any derivative $\frac{\partial}{\partial x_i}$ can be written $\frac{\partial}{\partial x_i} = \xi_i \frac{d}{dn}$ + tangential derivatives. To prove this last statement consider

$$\xi_i \frac{d}{dn} = \xi_i \xi_k \frac{\partial}{\partial x_k} = \xi_i^2 \frac{\partial}{\partial x_i} + \xi_i \xi_n \frac{\partial}{\partial x_n} \; ; \; n \neq i$$

$$= (1 - \xi_n \xi_n) \frac{\partial}{\partial x_i} + \xi_i \xi_n \frac{\partial}{\partial x_n}$$

$$= \frac{\partial}{\partial x_i} + (\xi_i \xi_n \frac{\partial}{\partial x_n} - \xi_n \xi_n \frac{\partial}{\partial x_i}) \qquad \text{(A-4)}$$

By using the above definitions it is easily shown that the term in parentheses in Eq. (A-4) is a tangential derivative.

Therefore, substituting for $\frac{\partial}{\partial x_i}$ in the Eulerian flow equations we get

$$(\xi_0 + \xi_i u_i) \frac{d\rho}{dn} + \rho \xi_i \frac{du_i}{dn} = \text{tangential derivatives}$$

$$(\xi_0 + \xi_i u_i) \frac{du_g}{dn} + \frac{\xi_g}{\rho} \frac{dp}{dn} = \text{tangential derivatives} \qquad \text{(A-5)}$$

$$(\xi_0 + \xi_i u_i) \frac{dp}{dn} - \frac{\gamma p}{\rho} (\xi_0 + \xi_i u_i) \frac{d\rho}{dn} = \text{tangential derivatives}$$

Equation (A-5) is an equation for the normal derivatives of the flow variables in terms of data which are prescribed on the surface $\phi(t, x_i)$. If the surface is a characteristic surface the set of Eqs. (A-5) cannot be solved for the normal derivatives $\frac{d\rho}{dn}, \frac{dp}{dn}, \frac{du_i}{dn}$ and the determinant of the coefficients equals zero. Taking the determinant and setting it equal to zero

$$(\xi_0 + \xi_i u_i)^3 ((\xi_0 + \xi_i u_i)^2 - a^2 (\xi_i \xi_i)) = 0 \qquad \text{(A-6)}$$

where $a^2 = \gamma p / \rho$

Using the definition of ξ_k given in (A-2), Eq. (A-6) leads to the following partial differential equations for the characteristic surfaces:

$$\phi_t + u_i \phi_{x_i} = 0 \qquad \text{(A-7)}$$

$$\phi_t + u_i \phi_{x_i} \pm a \sqrt{\phi_{x_i} \phi_{x_i}} = 0 \qquad \text{(A-8)}$$

Equation (A-7) is linear and represents a directional derivative $d\phi = \phi_t\, dt + \phi_{x_i}\, dx_i$ provided $\frac{dt}{1} = \frac{dx_i}{u_i}$ or $\frac{dx_i}{dt} = u_i$. That is, the surface $\phi(t, x_i) = \text{const.}$ along the streamlines, $\frac{dx_i}{dt} = u_i$. Hence the streamlines form a characteristic surface for the Eqs. (A-1). However we are more interested in the characteristic Eq. (A-8), this is discussed in Section II.